On the increase of climate sensitivity and cloud feedback with warming in the Community Atmosphere Models

Jiang Zhu[1,2*] & Christopher J. Poulsen[1]

[1]*Department of Earth and Environmental Sciences, University of Michigan, Ann Arbor, MI 48109*

[2]*Climate and Global Dynamics Laboratory, National Center for Atmospheric Research, Boulder, CO 80305*

Key Points:

- ECS increases with CO_2-induced global warming in CAM 6, 5, and 4, and is primarily attributed to the strengthening of cloud feedback.
- High-latitude λ_{cld} strengthens with warming due to a decrease of cloud ice fraction and a weakening of the negative cloud-phase feedback.
- Low-latitude λ_{cld} strengthening is linked to cloud thinning over subsidence regions likely caused by cloud interactions with water vapor.

*Corresponding to: Jiang Zhu (jiangzhu@ucar.edu)

Plain Language Summary: Equilibrium climate sensitivity (ECS) is defined as the equilibrium increase in global mean temperature as a result of a doubling of atmospheric CO_2 concentration. The latest assessment by the Intergovernmental Panel on Climate Change reported a likely ECS range of 1.5–4.5°C. Narrowing the ECS range is of paramount importance for prediction of future warming. Earth's surface has experienced prolonged periods of large magnitude warming in the geological past, which provide important empirical information on ECS. To quantitatively use the paleoclimate information, we need a complete understanding of how ECS may depend on the background climate. In this study, we investigate the physical mechanisms responsible for the state dependence of ECS using three climate models that have distinct model physics. In all three models, we find that ECS grows as the background climate warms, i.e., a warmer climate is more sensitive to external forcing. We attribute the increase of ECS to both high- and low-latitude cloud processes. Over high latitudes, cloud ice fraction decreases with global warming, weakening the potential for mixed-phase clouds to reflect solar radiation and amplifying surface warming. Over low latitudes, global warming enhances the efficiency of processes that make clouds less opaque, again, amplifying surface warming.

Abstract: Modeling and paleoclimate proxy-based studies suggest that equilibrium climate sensitivity (ECS) depends on the background climate state, though the reason is not thoroughly understood. Here we study the state dependence of ECS over a large range of global mean surface temperature (GMST) in the Community Atmosphere Model (CAM) versions 4, 5, and 6 by varying atmospheric CO_2 concentrations. We find a robust increase of ECS with GMST in all three models, albeit at different rates, which is primarily attributed to strengthening of the shortwave cloud feedback (λ_{cld}) at both high and low latitudes. Over high latitudes, increasing GMST leads to a reduction in the cloud ice fraction, weakening the (negative) cloud-phase feedback due to the phase transition of cloud ice to liquid and thereby strengthening λ_{cld}. Over low-latitude regions, increasing GMST strengthens λ_{cld} likely through the nonlinear increase in water vapor, which causes low-cloud thinning through thermodynamic and radiative processes.

1. Introduction

ECS, defined as the equilibrium GMST increase to the radiative forcing caused by a doubling of atmospheric CO_2 concentrations, is an important metric of the severity of long-term climate change (e.g., Knutti, Rugenstein, & Hegerl, 2017). Because of its importance for projecting future climate and for making effective policies and adaptation plans, a tremendous effort has been made to quantify ECS since the 1960s (e.g., Manabe & Wetherald, 1967). Despite these efforts, ECS is still loosely constrained with a 'likely' range of 1.5–4.5°C that has remained essentially unchanged for 40 years (Charney et al., 1979; IPCC, 2013). ECS estimates from individual studies have a much larger range from ~1°C to more than 10°C depending on methods, models, and time periods of interest (Knutti et al., 2017). Studies using global climate models (GCMs) increasingly suggest that ECS depends on the background climate, which may partly explain the large range of ECS estimates in individual studies (Caballero & Huber, 2013; Colman & McAvaney, 2009; Hansen, Sato, Russell, & Kharecha, 2013; Jonko, Shell, Sanderson, & Danabasoglu, 2013; Kutzbach, He, Vavrus, & Ruddiman, 2013; Mauritsen et al., 2019; Meraner, Mauritsen, & Voigt, 2013; Wolf, Haqq-Misra, & Toon, 2018; Zhu, Poulsen, & Tierney, 2019).

The large spread of pre-industrial (PI) climate ECS among GCMs has been attributed to uncertainties in the cloud feedback, which either amplifies or dampens the surface temperature response through changes in cloud radiative effects (Bony & Dufresne, 2005; Cess et al., 1990; Soden & Held, 2006; Zelinka et al., 2020). Modeling studies focusing on background climates other than PI suggest that the cloud feedback increases with GMST and contributes to the increase of ECS with global warming (Caballero & Huber, 2013; Hansen et al., 2013; Jonko et al., 2013; Mauritsen et al., 2019; Meraner et al., 2013; Wolf et al., 2018; Zhu et al., 2019). In particular, an abrupt rise in the cloud feedback and ECS was reported in an Early Eocene simulation using the Community Climate System Model (CCSM3) when GMST exceeded ~23°C (CO_2 > 1120 ppmv) (Caballero & Huber, 2013). In contrast, a recent Early Eocene simulation using the Community Earth System Model (CESM1.2, an updated version of CCSM3) showed continuous and larger increases in the cloud feedback and ECS with warming with no apparent threshold in GMST or CO_2 concentrations (Zhu et al., 2019). The mechanism responsible for the increase in cloud feedback with global temperature in these GCM studies has not been thoroughly investigated (Caballero & Huber, 2013; Mauritsen et al., 2019; Meraner et al., 2013; Zhu et al., 2019).

In this study, we explore the state dependence of ECS and cloud feedback across a large range of CO_2 levels in CAM versions 4, 5, and 6 within the framework of CESM. We analyze the state dependence of the cloud feedback through a decomposition of cloud regimes and cloud feedback components, and through a comparison between CAM versions.

2. Models, experiments, and methods

CAM 4, 5, and 6 within CESM are state-of-the-art models that have participated in the latest two phases of the Coupled Model Intercomparison Project (Danabasoglu et al., 2020; Hurrell et al., 2013). CAM5 differs from CAM4 in the physical parameterizations of radiation, boundary layer and shallow convection, aerosol, and cloud microphysics and macrophysics, with only the deep convection scheme unchanged (Hurrell et al., 2013). In CAM6, the boundary layer, shallow convection, and warm cloud macrophysics schemes have been replaced with the Cloud Layers Unified by Binormals parameterization (Gettelman et al., 2019). The two-moment microphysics scheme has been implemented for both stratiform and shallow convective clouds in

CAM6, in contrast to only stratiform clouds in CAM5. Due to these changes in physical parameterizations, CAM has made progressive improvements in cloud simulation when compared with satellite observations (Gettelman et al., 2019; Jiang et al., 2012; Kay et al., 2012; Klein et al., 2013). In slab ocean simulations (SOM) under modern conditions, ECS increases from 3.1°C in CAM4 to 4.2°C in CAM5 and to ~5.3°C in CAM6. The increasing ECS in CAM versions has been attributed to the updated radiation scheme and a strengthening of the positive cloud feedback due to improvements in the representation of cloud processes (Gettelman et al., 2019; Gettelman, Kay, & Shell, 2012).

To gain insights into the state-dependence of ECS and the cloud feedback, we performed SOM simulations with various atmospheric CO_2 levels. CAM6 simulations were carried out with 1, 2, and 4× the PI CO_2 level (PIC; 284.7 ppmv); CAM5 simulations with 1, 2, 4, 8, and 12× PIC; and, CAM4 simulations with 1, 2, 4, 8, 16, and 32× PIC to cover a comparable range in GMST. Model instability in CAM6 8× and CAM5 16× experiments prevented us from finishing those simulations; instead, we conducted a CAM5 12× case. Each set of SOM simulations employ identical non-CO_2 PI boundary conditions, and mixed layer depths and heat transport convergence derived from corresponding fully coupled PI simulations with a dynamic ocean. To be consistent with the corresponding fully coupled simulations, CAM4 and CAM5 SOM simulations were run with a horizontal resolution of 1.9° × 2.5° (latitude × longitude) and CAM6 with a resolution of 0.9° × 1.25°. In CESM2, CAM6 is coupled with updated versions of land and sea ice models, which do not impact the climate sensitivity (Gettelman et al., 2019). All SOM simulations were run for 60 model years. ECS for each climate state/CO_2 level is obtained by subtracting the final 20-year mean GMST in a SOM simulation from a corresponding one with twice the CO_2 level (e.g. $ECS_{2\times} = GMST_{4\times} - GMST_{2\times}$). The GMST range (up to ~30°C) covered in these simulations is broadly comparable to paleoclimate temperatures over the Cenozoic Era of Earth history (the past 66 million years).

To quantify the cloud feedback, we calculated the cloud feedback parameter (λ_{cld}) using a two-way partial radiative perturbation (PRP) method (Colman, 2003; Zhu et al., 2019). We did not use radiative kernels because they were mostly developed for the present-day climate and their assumption of linearity may be violated under a large forcing (Jonko et al., 2013). Our PRP method used offline radiation calculations driven by 10 years of high frequency instantaneous radiation fields in CAM4 and CAM5, and 3 years of radiation fields in CAM6 due to the higher horizontal resolution and greater storage demand. We performed PRP analysis for three pairs of CO_2 experiments in CAM4 (1→2×, 4→8×, and 16→32×) and CAM5 (1→2×, 4→8×, and 8→12×), and two pairs in CAM6 (1→2× and 2→4×). Additional PRP analyses were not feasible due to the large storage and computational cost of the analysis. Instead, we performed approximate PRP (APRP) analyses for all the simulations to quantify the shortwave λ_{cld} and its decomposition into contributions from changes in cloud amount, scattering, and absorption (Taylor et al., 2007). APRP is much less expensive and produces satisfactory results with differences from PRP less than 7% (Taylor et al., 2007; see also Figure 2 and Table S1). To further understand λ_{cld} variations, we implemented a PRP-based decomposition method to quantify the contribution from changes in individual cloud properties in CAM5 (Zhu & Poulsen, 2019), e.g., the phase partitioning of cloud water between ice and liquid. We defer similar PRP-based decomposition in CAM6 and CAM4 to future work due to our limited computing and storage resources. Readers are referred to Zhu and Poulsen (2019) for details on the implementation of the PRP method.

3. Results

3.1 Increases of ECS and λ_{cld} with warming

CAM 4, 5, and 6 predict GMSTs of ~15°C in their PI simulations (1×; Figure 1a). Under higher CO_2 levels, CAM versions exhibit large inter-model differences in GMST. For example, under 4× PIC, CAM6 simulates a GMST of 27.6°C, which is 4.3 and 6.5°C higher than that in CAM5 and CAM4, respectively. Inter-model differences in warming are much greater at regional scales, exceeding 10°C over mid-latitude continents and the Arctic Ocean (Figure S1).

CAM 4, 5, and 6 all exhibit increases of ECS with global warming but at different rates (Figure 1b). CAM6 ECS increases from the PI value of 5.5°C to 6.9°C under a warmer climate with 2× PIC. CAM5 exhibits a gradual increase in ECS with warming, rising from 4.2 to 4.6 and 5.4°C for the first, second and third CO_2 doubling, respectively. In contrast, CAM4 ECS is initially stable with values of ~3.2–3.4°C when GMST is below ~23°C (CO_2 below 4× PIC) and exhibits substantial increases of 20–60% to 3.9 and 5.1°C at 8 and 16× PIC, respectively.

λ_{cld} variations between CAM versions and their dependence on GMST in each model closely follow the ECS changes (Figure 1c; see Table S1 for values with uncertainty and a comparison between results using PRP and APRP). Similar to the increase of CAM6 ECS with CO_2-induced warming, λ_{cld} in CAM6 increases from 0.97±0.03 (1σ) in 1× to 1.07±0.02 W m^{-2} K^{-1} in 2× PIC. CAM5 λ_{cld} increases gradually with the background warming from 0.60±0.05 to 0.79±0.04 and to 1.03±0.02 W m^{-2} K^{-1} in 1, 4, and 8× PIC (calculated using 8 and 12×), respectively. CAM4 λ_{cld} values are 0.15±0.12 and 0.21±0.07 W m^{-2} K^{-1} in background states of 1 and 4× PIC, respectively, and exhibit a substantial increase to 0.37±0.05 W m^{-2} K^{-1} at 16×PIC. The overall increases of λ_{cld} with warming in CAM5 and CAM4 are consistent with previous Eocene simulations that used similar models and covered a comparable GMST range (Caballero

& Huber, 2013; Zhu, Poulsen, & Otto-Bliesner, 2020; Zhu et al., 2019). Overall, the majority of the λ_{cld} increase in CAM versions is attributable to increases in the shortwave component (Figure 1c).

Increases in ECS with GMST in these experiments are primarily attributed to the cloud feedback. Using a bulk estimation method (e.g., Zelinka et al., 2020), we calculate a hypothetical ECS that would exist if the cloud feedback changed but the radiative forcing and non-cloud feedbacks were kept unchanged (Text S1 and Table S2). Our results suggest that increases in λ_{cld} explain ~70% (~1°C) of the total ECS increases in these simulations. The remaining ECS changes are attributable to non-cloud feedbacks and enhancements of the efficacy of CO_2 radiative forcing (Byrne & Goldblatt, 2014; Caballero & Huber, 2013; Hansen et al., 2005; Meraner et al., 2013; Zhu et al., 2019). The predominance of λ_{cld} in driving the state dependence of ECS is consistent with complete forcing-feedback analyses in previous simulations of past warm climates (Caballero & Huber, 2013; Zhu et al., 2019).

3.2 λ_{cld} decomposition into cloud regimes and components

To understand its state dependence, we broadly divide λ_{cld} into three cloud regimes: high-latitude (λ_{cld_hlat}; 30–90°S/N), low-latitude subsidence (λ_{cld_subs}; 30°S–30°N and $\omega_{500} > 0$), and low-latitude ascending (λ_{cld_asce}; 30°S–30°N and $\omega_{500} < 0$). Monthly mean 500-hPa vertical velocity (ω_{500}) is used to distinguish low-latitude ascending and subsidence regimes (Bony & Dufresne, 2005). Our cloud regime division is based on the understanding that cloud feedback processes are complex and exhibit distinct spatial patterns (Ceppi, Brient, Zelinka, & Hartmann, 2017; Gettelman & Sherwood, 2016): λ_{cld_hlat} is mostly impacted by storm dynamics and thermodynamic changes in cloud water content and phase; λ_{cld_asce} is primarily controlled by tropical radiative-convective processes; and λ_{cld_subs} is determined by the complicated interplay between radiation, boundary layer turbulence, convection, and large-scale dynamics. The extent of individual cloud regimes varies little in our simulations (Table S3), such that their contribution to the global mean λ_{cld} primarily reflects changes in the magnitude of λ_{cld} over individual regimes, not their spatial coverage. In the following analysis, we weight λ_{cld} over individual regimes by their fractional area coverage, such that summing over regimes recovers the global mean λ_{cld}.

Over high latitudes, CAM5 and CAM6 show an increase of λ_{cld_hlat} with GMST that originates primarily from the shortwave component (Figure 2a–c). In CAM5, the shortwave λ_{cld_hlat} initially increases by ~0.14 W m^{-2} K^{-1} with warming from 14.4 to 23.3°C (1 to 4× PIC) and appears to nearly saturate at higher GMSTs. CAM6 exhibits a slightly larger shortwave λ_{cld_hlat} increase with warming from 15.2 to 20.8°C (1 to 2× PIC). Due to an instability in CAM6 at higher GMSTs, we are not able to determine whether shortwave λ_{cld_hlat} saturates with additional warming as in CAM5. APRP decomposition suggests that the shortwave λ_{cld_hlat} increases in CAM5 and CAM6 are dominated by changes in cloud scattering (Figure 2d) rather than cloud amount (Figure 2e). CAM4 cloud-scattering feedback also increases with warming but at a much smaller rate and saturates at a lower GMST (Figure 2d).

Over the low-latitude ascending regime, CAM 4, 5, and 6 exhibit remarkable inter-model consistency in the increase of longwave λ_{cld_asce} with GMST (~0.01 W m^{-2} K^{-1} per K of global warming; Figure 2g). This strengthening of longwave λ_{cld_asce} likely reflects nonlinear lifting of the tropical deep convective clouds with warming that is driven by radiative cooling of water vapor within the framework of radiative convective equilibrium and the fixed anvil temperature hypothesis (Hartmann & Larson, 2002). The shortwave $\lambda_{\mathrm{cld\_asce}}$ exhibits much less inter-model consistency (Figure 2h).

Over the low-latitude subsidence regime, both CAM4 and CAM5 exhibit a $\lambda_{\mathrm{cld\_subs}}$ increase in excess of 0.1 W m^{-2} K^{-1} when background GMSTs increase from ~20–23°C to ~29°C (Figure 2k). The $\lambda_{\mathrm{cld\_subs}}$ increase is from the shortwave component, with a greater increase in CAM4 shortwave that is partly compensated by a larger decrease in the longwave feedback (Figure 2l,m). APRP decomposition suggests that the shortwave $\lambda_{\mathrm{cld\_subs}}$ increase is primarily caused by changes in cloud scattering (Figure 2n), i.e. clouds become increasingly thinner with warming in both CAM4 and CAM5. With background GMSTs below ~20–23°C, CAM5 and CAM6 show a decrease of shortwave $\lambda_{\mathrm{cld\_subs}}$ with warming, which is insignificant in CAM4 (Figure 2m). The shortwave $\lambda_{\mathrm{cld\_subs}}$ decrease at lower GMSTs is associated with small reductions in both cloud amount and scattering feedbacks (Figure 2m–o).

4. Discussion

Model physical parameterizations differ substantially among CAM versions (Danabasoglu et al., 2020; Hurrell et al., 2013); nevertheless, some aspects of the temperature dependence in λ_{cld} are remarkably consistent between models. We suggest that inter-model consistent behaviors likely result from basic physical mechanisms that are largely independent of the details of the physical parameterizations, and therefore more robust. We next discuss such mechanisms.

4.1 High-latitude cloud-phase feedback

The phase transition from cloud ice to liquid likely explains most of the temperature dependence of $\lambda_{\mathrm{cld\_hlat}}$ in CAM5. In comparison to ice, liquid clouds reflect more shortwave radiation because liquid droplets are much smaller in size and precipitate less efficiently than ice crystals (Pruppacher & Klett, 1997). The phase transition of cloud ice to liquid constituents a negative cloud-phase feedback (Mitchell, Senior, & Ingram, 1989) that weakens with temperature increase (Tan, Storelvmo, & Zelinka, 2016). We quantified this cloud-phase feedback in CAM5 simulations using a PRP-based approach (Zhu & Poulsen, 2019). As expected, in response to the warming induced by the first CO_2 doubling (1→2×) in CAM5, the shortwave cloud-phase feedback is negative and lowest in the Southern Ocean (~–1.5 W m^{-2} K^{-1}) and the Northern Hemisphere mid- and high-latitudes (–0.2—0.6 W m^{-2} K^{-1}) (Figure 3c; longwave component is small and not shown). As the climate warms, the overall cloud ice fraction decreases (Figure 3a,b) and the mixed-phase clouds shift to higher altitude. In response to the third CO_2 doubling (4→8×) in CAM5, the cloud-phase feedback weakens over most of the mid- and high-latitudes to values higher than –0.4 W m^{-2} K^{-1} (Figure 3d). The weakening of the cloud-phase feedback contributes an increase of 0.11 W m^{-2} K^{-1} to changes in the global mean λ_{cld}, explaining ~80% of its temperature dependence below a GMST of ~23°C (4× PIC). This result indicates that other relevant processes, such as the dynamical poleward shift of storm tracks (Grise & Polvani, 2014), the thermodynamic increase of cloud water content with temperature (Betts & Harshvardhan, 1987), and changes in cloud particle size (Zhu & Poulsen, 2019), are overall less temperature dependent or they cancel with each other.

In CAM5, the PI cloud-phase feedback of –1.5 W m^{-2} K^{-1} over the Southern Ocean is much larger than observation-based estimates (McCoy, Hartmann, & Grosvenor, 2014), which is consistent with the well-known fact that CAM5 has insufficient amounts of supercooled liquid in mixed-phase clouds (too much cloud ice) (Frey & Kay, 2018; Kay et al., 2016). Although the cloud-phase feedbacks have not yet been quantified in CAM4 and CAM6, we expect that they exhibit a similar overall weakening with warming based on basic thermodynamics (Tan et al., 2016). Details of the cloud-phase feedback (e.g. rates of change with warming and the saturation temperature) should depend on the microphysical parameterizations of mixed-phase clouds (McCoy, Tan, Hartmann, Zelinka, & Storelvmo, 2016) and need future study.

4.2 Low-latitude cloud thinning

We hypothesize that the increase of λ_{cld_subs} with warming results from the exponential increase of water vapor (q) with GMST (the Clausius-Clapeyron relation; C-C relation) and the associated thermodynamic and radiative cloud thinning processes, i.e. the decrease in cloud optical thickness with warming. The thermodynamic mechanism involves a nonlinear temperature dependence in the moisture gradient (Δq) between the free troposphere (FT) and the planetary boundary layer (PBL). With the same amount of turbulent entrainment, a larger Δq means that relatively drier FT air is mixed into the PBL, producing thinner low clouds (Bretherton, 2015; van der Dussen, de Roode, Dal Gesso, & Siebesma, 2015). Recent studies have emphasized the role of Δq in regulating cloud-top entrainment and as a predictor for low clouds (Eastman & Wood, 2018; Kawai, Koshiro, & Webb, 2017). To demonstrate this mechanism, we examine Δq (defined here as $q_{1000hPa}$–q_{700hPa}) over the low-latitude subsidence regime using the concept of cloud-controlling factors (see Klein, Hall, Norris, & Pincus, 2017 for a review of cloud-controlling factors):

$$\lambda_{\mathrm{cld\_subs}} = \frac{\mathrm{dCRE}}{\mathrm{dGMST}} = \frac{\partial \mathrm{CRE}}{\partial \Delta \mathrm{q}} \frac{\mathrm{d}\Delta \mathrm{q}}{\mathrm{dGMST}} \qquad (1).$$

Equation (1) expresses that cloud radiative effects (CRE) respond to changes in Δq ($\frac{\partial \mathrm{CRE}}{\partial \Delta q} > 0$), which, in turn, is a function of GMST. Δq is enhanced by warming ($\frac{\mathrm{d}\Delta \mathrm{q}}{\mathrm{dGMST}} > 0$) because humidity increases at a higher rate within the PBL than the FT (Figure 4a), consistent with the C-C relation. CAM simulations further suggest that the nonlinear C-C relation yields a non-constant $\frac{d\Delta q}{d\mathrm{GMST}}$ that increases with GMST (Figure 4b), giving rise to a $\lambda_{\mathrm{cld\_subs}}$ increase with warming.

The radiative mechanism lies in the downwelling longwave radiation associated with the nonlinear increase of FT water vapor with GMST. Greater downwelling longwave radiation from the FT reduces cloud-top longwave cooling in the boundary layer, which weakens convection between the cloud layer and the surface and reduces the optical thickness of low clouds by decoupling them from their surface moisture supply (Bretherton, 2015; Schneider, Kaul, & Pressel, 2019). This radiative cloud thinning mechanism has been identified from satellite observations and large-eddy simulations (Bretherton, 2015; Christensen, Carrió, Stephens, & Cotton, 2013; Schneider et al., 2019), but is difficult to quantify within a GCM. Nevertheless, this mechanism is based on basic physics and intrinsically nonlinear, and appears to be consistent with the increase of $\lambda_{\mathrm{cld\_subs}}$ with warming in CAM4 and CAM5.

In addition to water vapor-related mechanisms, we have also examined other cloud-controlling factors including the estimated inversion strength (EIS; a metric for the lower-tropospheric stability; Figure 4c,d), the subsidence strength (Myers & Norris, 2013), and the surface wind speed (Bretherton, Blossey, & Jones, 2013) (Figure S2 and Text S2). A decrease in EIS enhances the mixing between the dry FT and the moist PBL, thinning low clouds ($\frac{\partial \mathrm{CRE}}{\partial \mathrm{EIS}} < 0$) (Wood & Bretherton, 2006). In CAM4 and CAM5, the sensitivity of EIS to GMST ($\frac{d\mathrm{EIS}}{d\mathrm{GMST}}$) initially weakens and then strengthens substantially with GMST increases (Figure 4a,b), resembling the temperature dependence of the shortwave $\lambda_{\mathrm{cld\_subs}}$ (Figure 2m,n). These results suggest that variations of the lower-tropospheric stability with warming may also contribute to the temperature-dependent $\lambda_{\mathrm{cld\_subs}}$ in CAM4 and CAM5. Additional analyses indicate that surface winds over the subsidence regime weaken with warming, likely contributing to the weakening of $\lambda_{\mathrm{cld\_subs}}$ below a GMST of ~20°C (Figure 2m–o; Figure S2 and Text S2) through decreasing latent heat fluxes (Bretherton, Blossey, & Jones, 2013).

We point out here that the cloud-controlling factors covary, making it difficult to conclusively compare their individual role in coupled processes. For example, the lower-tropospheric stability is largely controlled by the pattern of surface warming and, therefore, closely coupled with the cloud feedback (Ceppi & Gregory, 2017; Erfani & Burls, 2019). We note further that the state dependence of λ_{cld} could originate from the sensitivity of CRE on the cloud-controlling factors, which should depend on the details of model physical parameterizations (Klein et al., 2017). Further studies are needed to separate contributions from individual cloud-controlling factors and to investigate the nonlinearities in the dependence of CRE on the cloud-controlling factors, as well as the interactions of these cloud processes with dynamically evolving SST patterns.

5. Conclusions

In this study, we have explored ECS and the cloud feedback over a broad range of climate conditions by varying the atmospheric CO_2 concentrations in the latest three generations of CAM (versions 4, 5, and 6). Our simulations show that ECS and λ_{cld} increase with global warming in all three CAM versions and their inter-model differences become much larger at high CO_2 levels. In CAM6, ECS and λ_{cld} are 5.5°C and 0.97 W m^{-2} K^{-1} under preindustrial conditions, respectively, and they increase to 6.9°C and 1.07 W m^{-2} K^{-1} for the second CO_2 doubling. In

CAM5, ECS is 4.2°C under preindustrial conditions and increases gradually with GMST to 4.6 and 5.4°C for the second and third CO_2 doubling, respectively. Likewise, CAM5 λ_{cld} increases gradually from a preindustrial value of 0.60 to 0.79 W m^{-2} K^{-1} for the third CO_2 doubling. In CAM4, both ECS and λ_{cld} increases at GMSTs in excess of ~23°C (4× PIC) with ECS increasing from ~3°C to > 5°C and λ_{cld} from ~0.2 to ~0.4 W m^{-2} K^{-1}. λ_{cld} increases are dominated by the shortwave component and explain > 70% of the total ECS increases in the CAM simulations, suggesting a major role for the shortwave cloud feedback in setting the state dependence of ECS over a broad range of GMST.

We evaluate λ_{cld} over individual cloud regimes and identify robust temperature-dependent processes including (1) a high-latitude increase of shortwave λ_{cld} with warming when GMST < ~20–23°C, (2) a low-latitude increase of shortwave λ_{cld} with warming over the subsidence regime when GMST > ~20°C, and (3) a low-latitude increase of longwave λ_{cld} with warming over the ascending regime. Using a PRP-based λ_{cld} decomposition, we attribute ~80% of the high-latitude λ_{cld} increase in CAM5 to a weakening of the negative cloud-phase feedback, i.e., a decrease in the cloud glaciation rate with warming. The λ_{cld} increase over the low-latitude subsidence regime is hypothesized to be caused by the near exponential increase of water vapor with GMST, which leads to nonlinear cloud thinning through thermodynamic and radiative processes that should be largely independent of the details of the model physical parameterizations. The thermodynamic mechanism involves a nonlinear increase of the moisture gradient between the free troposphere and the PBL that enhances low-cloud thinning through mixing. The radiative mechanism involves the nonlinear increases of downwelling longwave radiation reaching cloud tops that suppresses convection and thins low clouds.

Acknowledgements: The authors thank Natalie Burls for helpful discussion and three anonymous reviewers for their constructive comments. This work was supported by Heising-Simons Foundation grant #2016-05 and #2016-12 and NSF grant 2002397 to C. Poulsen. CESM model code is available through the National Center for Atmospheric Research software development repository (https://svn-ccsm-models.cgd.ucar.edu/cesm1/release_tags/cesm1_2_2_1/) and the GitHub repository (https://github.com/ESCOMP/CESM/releases/tag/cesm2.1.1). Computing resources (doi:10.5065/D6RX99HX) were provided by the Climate Simulation Laboratory at NCAR's Computational and Information Systems Laboratory, sponsored by the National Science Foundation and other agencies. Relevant simulation data and results on the cloud feedback analysis will be published in the Zenodo repository (https://doi.org/ 10.5281/zenodo.3695929). Additional simulation data can be requested by contacting J.Z. (jiangzhu@ucar.edu).

References:

Betts, A. K., & Harshvardhan. (1987). Thermodynamic constraint on the cloud liquid water feedback in climate models. *Journal of Geophysical Research: Atmospheres, 92*(D7), 8483-8485. doi:10.1029/JD092iD07p08483

Bony, S., & Dufresne, J.-L. (2005). Marine boundary layer clouds at the heart of tropical cloud feedback uncertainties in climate models. *Geophysical Research Letters, 32*(20). doi:10.1029/2005GL023851

Bretherton, C. S. (2015). Insights into low-latitude cloud feedbacks from high-resolution models. *Philosophical Transactions of the Royal Society A: Mathematical, Physical and Engineering Sciences, 373*(2054). doi:10.1098/rsta.2014.0415

Bretherton, C. S., Blossey, P. N., & Jones, C. R. (2013). Mechanisms of marine low cloud sensitivity to idealized climate perturbations: A single-LES exploration extending the CGILS cases. *Journal of Advances in Modeling Earth Systems, 5*(2), 316-337. doi:10.1002/jame.20019

Byrne, B., & Goldblatt, C. (2014). Radiative forcing at high concentrations of well-mixed greenhouse gases. *Geophysical Research Letters, 41*(1), 152-160. doi:10.1002/2013gl058456

Caballero, R., & Huber, M. (2013). State-dependent climate sensitivity in past warm climates and its implications for future climate projections. *Proceedings of the National Academy of Sciences, 110*(35), 14162-14167. doi:10.1073/pnas.1303365110

Ceppi, P., Brient, F., Zelinka, M. D., & Hartmann, D. L. (2017). Cloud feedback mechanisms and their representation in global climate models. *WIREs Climate Change, 8*(4), e465. doi:10.1002/wcc.465

Ceppi, P., & Gregory, J. M. (2017). Relationship of tropospheric stability to climate sensitivity and Earth's observed radiation budget. *Proceedings of the National Academy of Sciences, 114*(50), 13126 LP-13131. doi:10.1073/pnas.1714308114

Cess, R. D., Potter, G. L., Blanchet, J. P., Boer, G. J., Del Genio, A. D., Déqué, M., . . . Zhang, M. H. (1990). Intercomparison and interpretation of climate feedback processes in 19 atmospheric general circulation models. *Journal of Geophysical Research: Atmospheres, 95*(D10), 16601-16615. doi:10.1029/JD095iD10p16601

Charney, J. G., Arakawa, A., Baker, D. J., Bolin, B., Dickinson, R. E., Goody, R. M., . . . Wunsch, C. I. (1979). *Carbon dioxide and climate: a scientific assessment*: National Academy of Sciences, Washington, DC.

Christensen, M. W., Carrió, G. G., Stephens, G. L., & Cotton, W. R. (2013). Radiative Impacts of Free-Tropospheric Clouds on the Properties of Marine Stratocumulus. *Journal of the Atmospheric Sciences, 70*(10), 3102-3118. doi:10.1175/JAS-D-12-0287.1

Colman, R. (2003). A comparison of climate feedbacks in general circulation models. *Climate Dynamics, 20*(7), 865-873. doi:10.1007/s00382-003-0310-z

Colman, R., & McAvaney, B. (2009). Climate feedbacks under a very broad range of forcing. *Geophysical Research Letters, 36*(1), L01702-L01702. doi:10.1029/2008GL036268

Danabasoglu, G., Lamarque, J.-F., Bacmeister, J., Bailey, D. A., DuVivier, A. K., Edwards, J., . . . Strand, W. G. (2020). The Community Earth System Model Version 2 (CESM2). *Journal of Advances in Modeling Earth Systems, 12*(2), e2019MS001916. doi:10.1029/2019ms001916

Eastman, R., & Wood, R. (2018). The Competing Effects of Stability and Humidity on Subtropical Stratocumulus Entrainment and Cloud Evolution from a Lagrangian

Perspective. *Journal of the Atmospheric Sciences*, *75*(8), 2563-2578. doi:10.1175/jas-d-18-0030.1

Erfani, E., & Burls, N. J. (2019). The Strength of Low-Cloud Feedbacks and Tropical Climate: A CESM Sensitivity Study. *Journal of Climate*, *32*(9), 2497-2516. doi:10.1175/JCLI-D-18-0551.1

Frey, W. R., & Kay, J. E. (2018). The influence of extratropical cloud phase and amount feedbacks on climate sensitivity. *Climate Dynamics, 50*(7), 3097-3116. doi:10.1007/s00382-017-3796-5

Gettelman, A., Hannay, C., Bacmeister, J. T., Neale, R. B., Pendergrass, A. G., Danabasoglu, G., . . . Mills, M. J. (2019). High Climate Sensitivity in the Community Earth System Model Version 2 (CESM2). *Geophysical Research Letters, 46*, 8329–8337. doi:10.1029/2019GL083978

Gettelman, A., Kay, J. E., & Shell, K. M. (2012). The Evolution of Climate Sensitivity and Climate Feedbacks in the Community Atmosphere Model. *Journal of Climate*, *25*(5), 1453-1469. doi:10.1175/JCLI-D-11-00197.1

Gettelman, A., & Sherwood, S. C. (2016). Processes Responsible for Cloud Feedback. *Current Climate Change Reports, 2*(4), 179-189. doi:10.1007/s40641-016-0052-8

Grise, K. M., & Polvani, L. M. (2014). Southern Hemisphere Cloud–Dynamics Biases in CMIP5 Models and Their Implications for Climate Projections. *Journal of Climate*, *27*(15), 6074-6092. doi:10.1175/JCLI-D-14-00113.1

Hansen, J., Sato, M., Ruedy, R., Nazarenko, L., Lacis, A., Schmidt, G. A., . . . Zhang, S. (2005). Efficacy of climate forcings. *Journal of Geophysical Research: Atmospheres*, *110*(D18104), 1-45. doi:10.1029/2005JD005776

Hansen, J., Sato, M., Russell, G., & Kharecha, P. (2013). Climate sensitivity, sea level and atmospheric carbon dioxide. *Philosophical Transactions of the Royal Society A: Mathematical, Physical and Engineering Sciences*, *371*(2001), 20120294. doi:10.1098/rsta.2012.0294

Hartmann, D. L., & Larson, K. (2002). An important constraint on tropical cloud - climate feedback. *Geophysical Research Letters*, *29*(20), 1951. doi:10.1029/2002GL015835

Hurrell, J. W., Holland, M. M., Gent, P. R., Ghan, S., Kay, J. E., Kushner, P. J., . . . Marshall, S. (2013). The community earth system model: A framework for collaborative research. *Bulletin of the American Meteorological Society*, *94*(9), 1339-1360. doi:10.1175/BAMS-D-12-00121.1

IPCC. (2013). *Climate Change 2013: The Physical Science Basis. Contribution of Working Group I to the Fifth Assessment Report of the Intergovernmental Panel on Climate Change* (T. F. Stocker, D. Qin, G.-K. Plattner, M. M. B. Tignor, S. K. Allen, J. Boschung, A. Nauels, Y. Xia, V. Bex, & P. M. Midgley Eds.). Cambridge, United Kingdom and New York, NY, USA.: Cambridge University Press.

Jiang, J., H., Su, H., Zhai, C., Perun Vincent, S., Del Genio, A., Nazarenko Larissa, S., . . . Stephens Graeme, L. (2012). Evaluation of cloud and water vapor simulations in CMIP5 climate models using NASA “A-Train” satellite observations. *Journal of Geophysical Research: Atmospheres, 117*(D14). doi:10.1029/2011JD017237

Jonko, A. K., Shell, K. M., Sanderson, B. M., & Danabasoglu, G. (2013). Climate Feedbacks in CCSM3 under Changing CO2 Forcing. Part II: Variation of Climate Feedbacks and Sensitivity with Forcing. *Journal of Climate*, *26*(9), 2784-2795. doi:10.1175/JCLI-D-12-00479.1

Kawai, H., Koshiro, T., & Webb, M. J. (2017). Interpretation of Factors Controlling Low Cloud Cover and Low Cloud Feedback Using a Unified Predictive Index. *Journal of Climate, 30*(22), 9119-9131. doi:10.1175/JCLI-D-16-0825.1

Kay, J. E., Hillman, B. R., Klein, S. A., Zhang, Y., Medeiros, B., Pincus, R., . . . Ackerman, T. P. (2012). Exposing Global Cloud Biases in the Community Atmosphere Model (CAM) Using Satellite Observations and Their Corresponding Instrument Simulators. *Journal of Climate, 25*(15), 5190-5207. doi:10.1175/JCLI-D-11-00469.1

Kay, J. E., Wall, C., Yettella, V., Medeiros, B., Hannay, C., Caldwell, P., & Bitz, C. (2016). Global Climate Impacts of Fixing the Southern Ocean Shortwave Radiation Bias in the Community Earth System Model (CESM). *Journal of Climate, 29*(12), 4617-4636. doi:10.1175/JCLI-D-15-0358.1

Klein, S. A., Hall, A., Norris, J. R., & Pincus, R. (2017). Low-Cloud Feedbacks from Cloud-Controlling Factors: A Review. *Surveys in Geophysics, 38*(6), 1307-1329. doi:10.1007/s10712-017-9433-3

Klein, S. A., Zhang, Y., Zelinka, M. D., Pincus, R., Boyle, J., & Gleckler, P. J. (2013). Are climate model simulations of clouds improving? An evaluation using the ISCCP simulator. *Journal of Geophysical Research: Atmospheres, 118*(3), 1329-1342. doi:10.1002/jgrd.50141

Knutti, R., Rugenstein, M. A. A., & Hegerl, G. C. (2017). Beyond equilibrium climate sensitivity. *Nature Geoscience, 10*, 727-727. doi:10.1038/ngeo3017

Kutzbach, J. E., He, F., Vavrus, S. J., & Ruddiman, W. F. (2013). The dependence of equilibrium climate sensitivity on climate state: Applications to studies of climates colder than present. *Geophysical Research Letters*, *40*(14), 3721–3726. doi:10.1002/grl.50724

Manabe, S., & Wetherald, R. T. (1967). Thermal Equilibrium of the Atmosphere with a Given Distribution of Relative Humidity. *Journal of the Atmospheric Sciences, 24*(3), 241-259. doi:10.1175/1520-0469(1967)024%3C0241:TEOTAW%3E2.0.CO

Mauritsen, T., Bader, J., Becker, T., Behrens, J., Bittner, M., Brokopf, R., . . . Roeckner, E. (2019). Developments in the MPI-M Earth System Model version 1.2 (MPI-ESM1.2) and Its Response to Increasing CO2. *Journal of Advances in Modeling Earth Systems*, *11*(4), 998-1038. doi:10.1029/2018MS001400

McCoy, D. T., Hartmann, D. L., & Grosvenor, D. P. (2014). Observed Southern Ocean Cloud Properties and Shortwave Reflection. Part II: Phase Changes and Low Cloud Feedback. *Journal of Climate, 27*(23), 8858-8868. doi:10.1175/JCLI-D-14-00288.1

McCoy, D. T., Tan, I., Hartmann, D. L., Zelinka, M. D., & Storelvmo, T. (2016). On the relationships among cloud cover, mixed-phase partitioning, and planetary albedo in GCMs. *Journal of Advances in Modeling Earth Systems*, *8*(2), 650-668. doi:10.1002/2015MS000589

Meraner, K., Mauritsen, T., & Voigt, A. (2013). Robust increase in equilibrium climate sensitivity under global warming. *Geophysical Research Letters, 40*(22), 5944-5948. doi:10.1002/2013GL058118

Mitchell, J. F. B., Senior, C. A., & Ingram, W. J. (1989). CO2 and climate: a missing feedback? *Nature, 341*(6238), 132-134. doi:10.1038/341132a0

Myers, T. A., & Norris, J. R. (2013). Observational Evidence That Enhanced Subsidence Reduces Subtropical Marine Boundary Layer Cloudiness. *Journal of Climate*, *26*(19), 7507-7524. doi:10.1175/jcli-d-12-00736.1

Pruppacher, H. R., & Klett, J. D. (1997). *Microphysics of Clouds and Precipitation* (second ed.). Boston, MA: Kluwer Academic Publishers.

Schneider, T., Kaul, C. M., & Pressel, K. G. (2019). Possible climate transitions from breakup of stratocumulus decks under greenhouse warming. *Nature Geoscience, 12*(3), 163-167. doi:10.1038/s41561-019-0310-1

Soden, B. J., & Held, I. M. (2006). An Assessment of Climate Feedbacks in Coupled Ocean–Atmosphere Models. *Journal of Climate, 19*(14), 3354-3360. doi:10.1175/JCLI3799.1

Tan, I., Storelvmo, T., & Zelinka, M. D. (2016). Observational constraints on mixed-phase clouds imply higher climate sensitivity. *Science*, *352*(6282), 224. doi:10.1126/science.aad5300

Taylor, K. E., Crucifix, M., Braconnot, P., Hewitt, C. D., Doutriaux, C., Broccoli, A. J., . . . Webb, M. J. (2007). Estimating Shortwave Radiative Forcing and Response in Climate Models. *Journal of Climate, 20*(11), 2530-2543. doi:10.1175/JCLI4143.1

van der Dussen, J. J., de Roode, S. R., Dal Gesso, S., & Siebesma, A. P. (2015). An LES model study of the influence of the free tropospheric thermodynamic conditions on the stratocumulus response to a climate perturbation. *Journal of Advances in Modeling Earth Systems, 7*(2), 670-691. doi:10.1002/2014MS000380

Wolf, E. T., Haqq-Misra, J., & Toon, O. B. (2018). Evaluating Climate Sensitivity to CO2 Across Earth's History. *Journal of Geophysical Research: Atmospheres, 123*(21), 11,861-811,874. doi:10.1029/2018JD029262

Wood, R., & Bretherton, C. S. (2006). On the Relationship between Stratiform Low Cloud Cover and Lower-Tropospheric Stability. *Journal of Climate, 19*(24), 6425-6432. doi:10.1175/JCLI3988.1

Zelinka, M. D., Myers, T. A., McCoy, D. T., Po-Chedley, S., Caldwell, P. M., Ceppi, P., . . . Taylor, K. E. (2020). Causes of Higher Climate Sensitivity in CMIP6 Models. *Geophysical Research Letters, 47*(1), e2019GL085782. doi:10.1029/2019GL085782

Zhu, J., & Poulsen, C. J. (2019). Quantifying the Cloud Particle-Size Feedback in an Earth System Model. *Geophysical Research Letters, 46*, 10910–10917. doi:10.1029/2019GL083829

Zhu, J., Poulsen, C. J., & Otto-Bliesner, B. L. (2020). High climate sensitivity in CMIP6 model not supported by paleoclimate. *Nature Climate Change*. doi:10.1038/s41558-020-0764-6

Zhu, J., Poulsen, C. J., & Tierney, J. E. (2019). Simulation of Eocene extreme warmth and high climate sensitivity through cloud feedbacks. *Science Advances, 5*(9), eaax1874. doi:10.1126/sciadv.aax1874

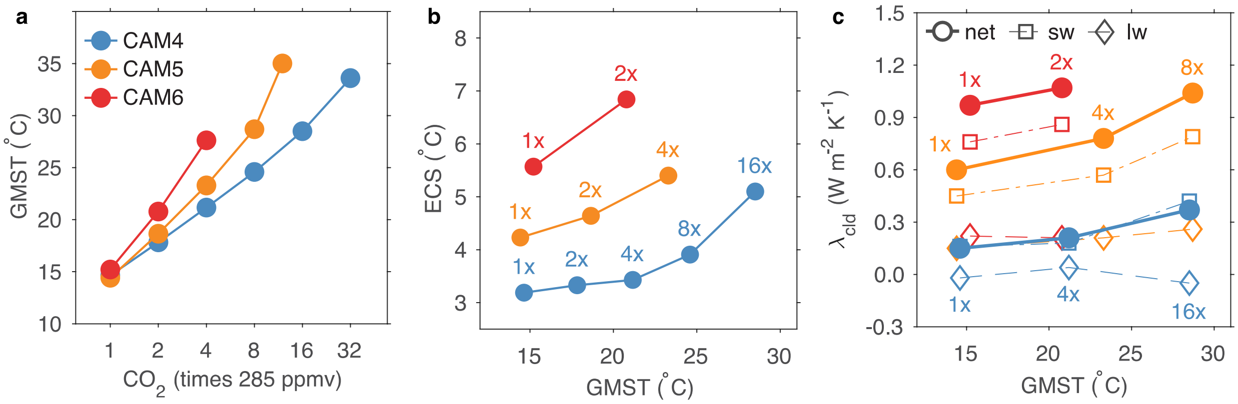

Figure 1. (**a**) GMST as a function of the atmospheric CO_2 concentration in SOM simulations using CAM 4, 5, and 6. (**b**) ECS and (**c**) λ_{cld} as a function of GMST. λ_{cld} (filled circles in **c**) is decomposed into shortwave (open squares) and longwave (open diamonds) components. Note that blue open squares (shortwave λ_{cld} for CAM4) lie behind the blue filled circles (total λ_{cld} for CAM4) in (**c**). The PRP analysis was performed for three pairs of CO_2 experiments in both CAM4 and CAM5, and two pairs in CAM6. CO_2 concentrations (in times preindustrial value) are listed in (**b**) and (**c**). The standard deviation of λ_{cld} is approximately 0.10 W m^{-2} K^{-1} in CAM4 and less than 0.05 W m^{-2} K^{-1} in CAM5 and CAM6; detailed numbers can be found in Table S1.

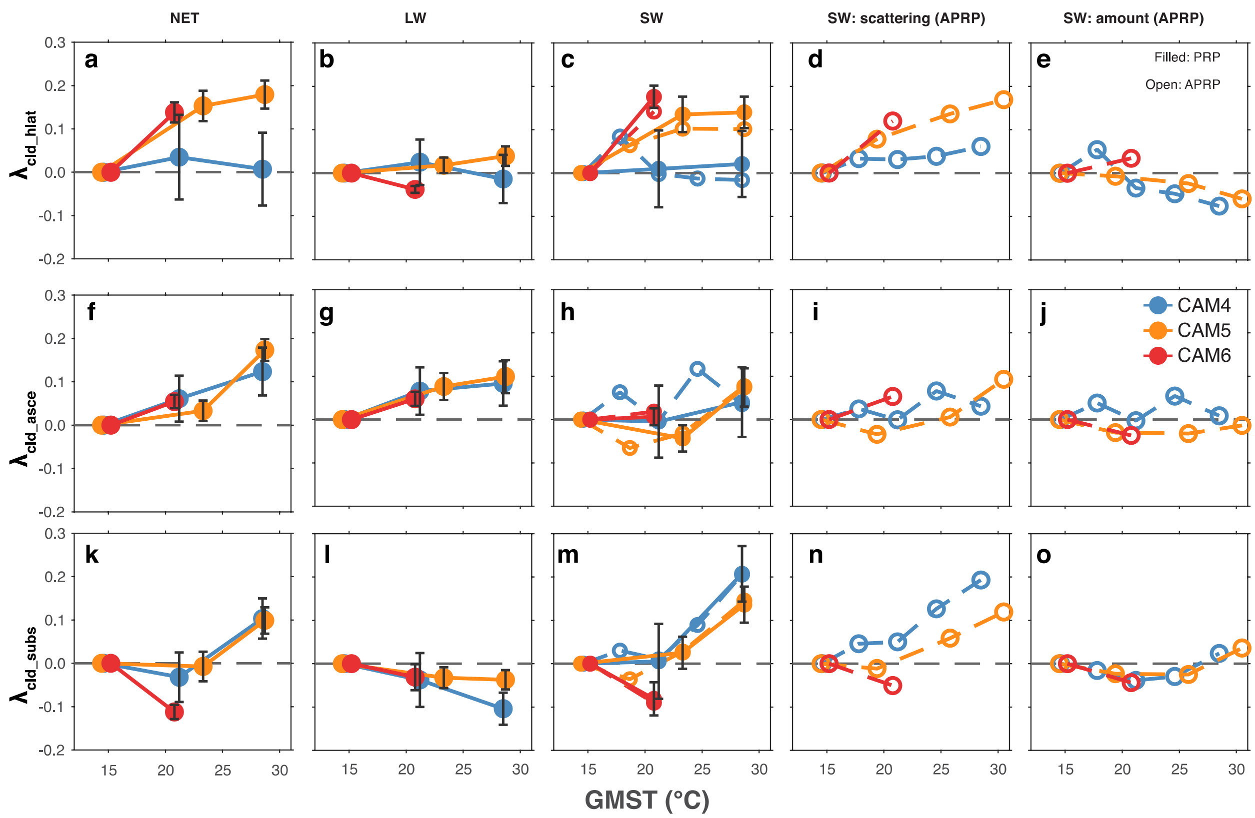

Figure 2. Changes in the cloud feedback parameter (λ_{cld}; units: W m^{-2} K^{-1}) relative to values under the preindustrial conditions. (**a**) λ_{cld} over the high-latitude regime (30–90°S/N; $\lambda_{\mathrm{cld\_hlat}}$) as a function of GMST in the simulations and its (**b**) longwave and (**c**) shortwave components. Using APRP, the shortwave λ_{cld} is further decomposed into contributions from changes in (**d**) cloud scattering and (**e**) amount. PRP and APRP results are shown as filled and open circles, respectively. (**f**)–(**j**) The same as (**a**)–(**e**), but for the low-latitude (30°S–30°N) ascending regime ($\lambda_{\mathrm{cld\_asce}}$). (**k**)–(**o**) The same as (**a**)–(**e**), but for the low-latitude (30°S–30°N) subsidence regime ($\lambda_{\mathrm{cld\_subs}}$). To compare the GMST dependence among models, λ_{cld} has been aligned based on their PI values and weighted by the area fraction of each cloud regime, such that summing over individual regimes recovers changes in global mean. Error bar in (**a**)–(**c**), (**f**)–(**h**), and (**k**)–(**m**) denotes the standard deviation in PRP analysis.

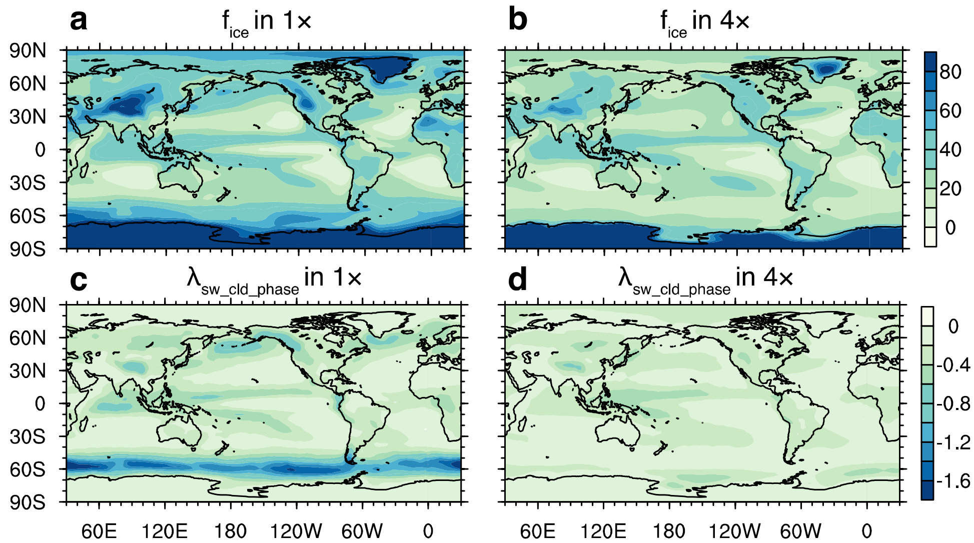

Figure 3. (**a**) Bulk cloud ice fraction (units: %) in CAM5 PI simulation. (**b**) The same as (**a**), but for simulation with 4× PIC. (**c**) The shortwave cloud-phase feedback (units: W m^{-2} K^{-1}) in CAM5 PI simulation. (**d**) The same as (**c**), but for simulation with 4× PIC.

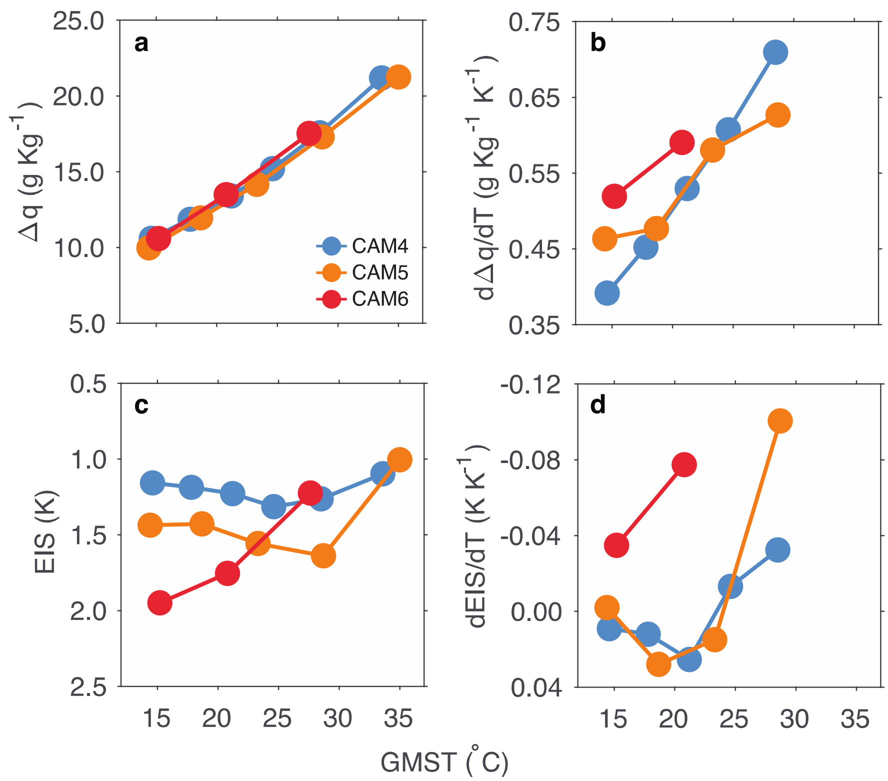

Figure 4. (**a**) Δq, the moisture gradient between the free troposphere and the PBL ($q_{1000hPa}$–q_{700hPa}), over the low-latitude subsidence regime as a function of GMST in the simulations. (**b**) The same as (**a**), but for $\frac{d\Delta q}{d\mathrm{GMST}}$, the sensitivity of Δq to GMST changes. (**c**) and (**d**) The same as (**a**) and (**b**), but for EIS. Note that vertical axes in (**c**) and (**d**) are reversed such that upward changes indicate a positive contribution to λ_{cld}.

Figure 1.

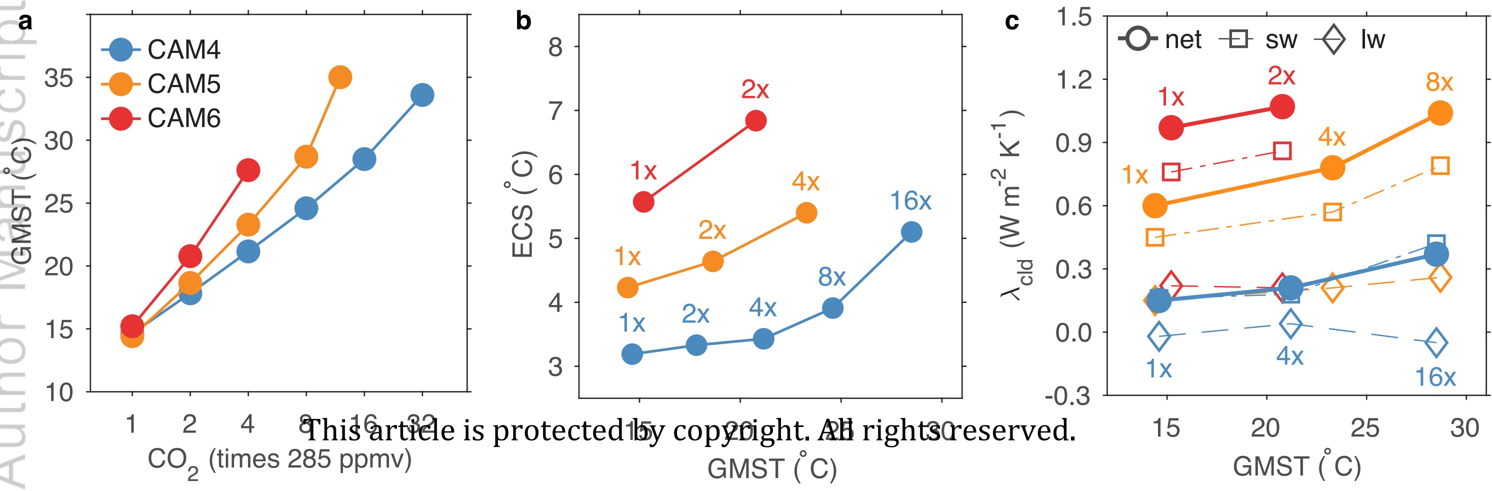
a
CAM4
CAM5
CAM6
GMST (°C)
35
30
25
20
15
10
1
2
4
8
16
32
CO2 (times 285 ppmv)
b
ECS (°C)
8
7
6
5
4
3
2x
1x
4x
2x
1x
16x
8x
1x
2x
4x
15
20
25
30
GMST (°C)
c
net
sw
lw
λcld (W m-2 K-1)
1.5
1.2
0.9
0.6
0.3
0.0
-0.3
1x
2x
8x
4x
1x
1x
4x
16x
15
20
25
30
GMST (°C)

Figure 2.

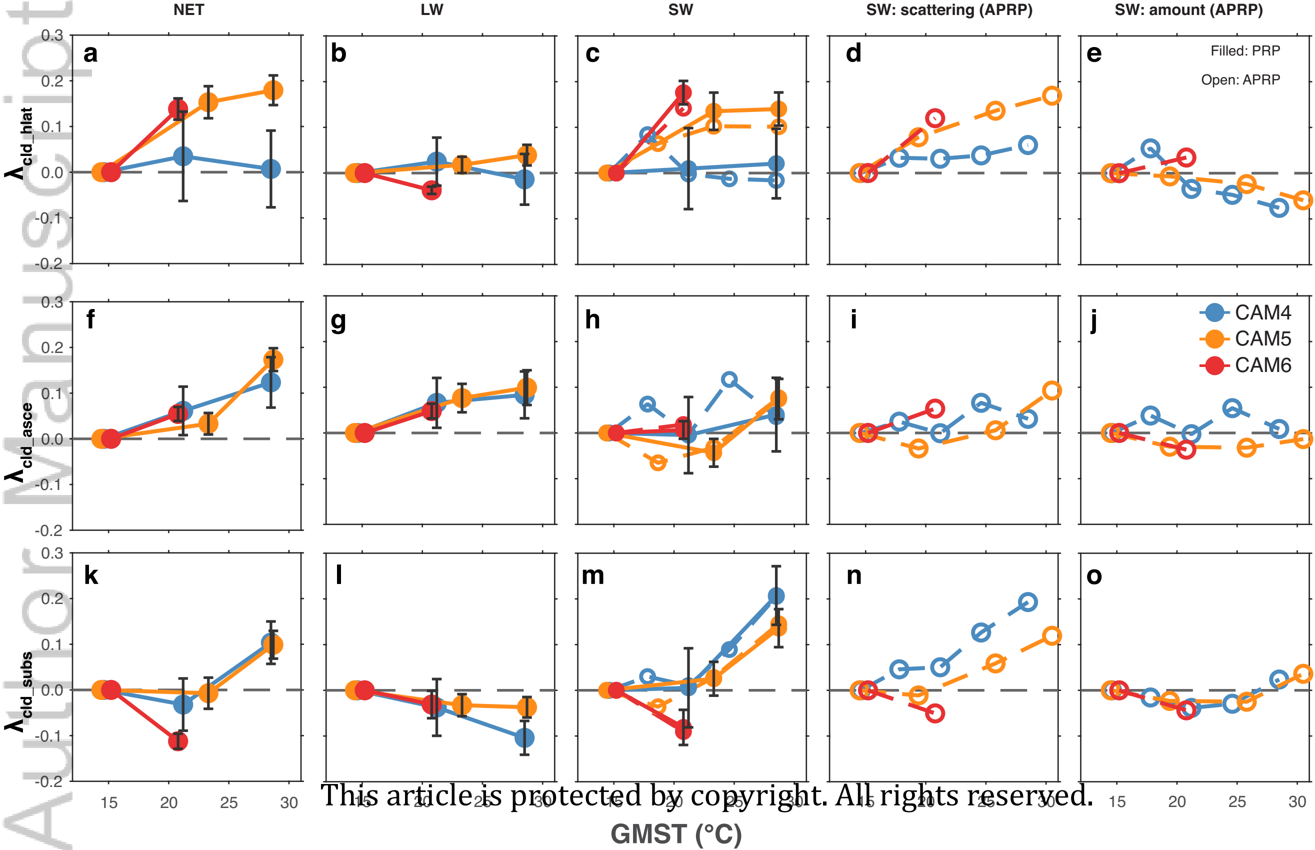

NET
LW
SW
SW: scattering (APRP)
SW: amount (APRP)
Filled: PRP
Open: APRP
CAM4
CAM5
CAM6
a
b
c
d
e
f
g
h
i
j
k
l
m
n
o
λ_{cld_hlat}
λ_{cld_asce}
λ_{cld_subs}
0.3
0.2
0.1
0.0
-0.1
-0.2
15
20
25
30
GMST (°C)

Figure 3.

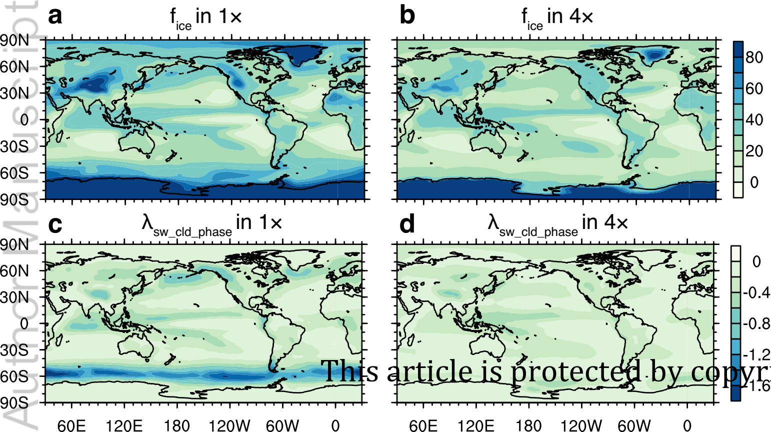

a
f_{ice} in 1×
b
f_{ice} in 4×
c
$\lambda_{sw\_cld\_phase}$ in 1×
d
$\lambda_{sw\_cld\_phase}$ in 4×
90N
60N
30N
0
30S
60S
90S
60E
120E
180
120W
60W
0
80
60
40
20
0
-0.4
-0.8
-1.2
-1.6

Figure 4.

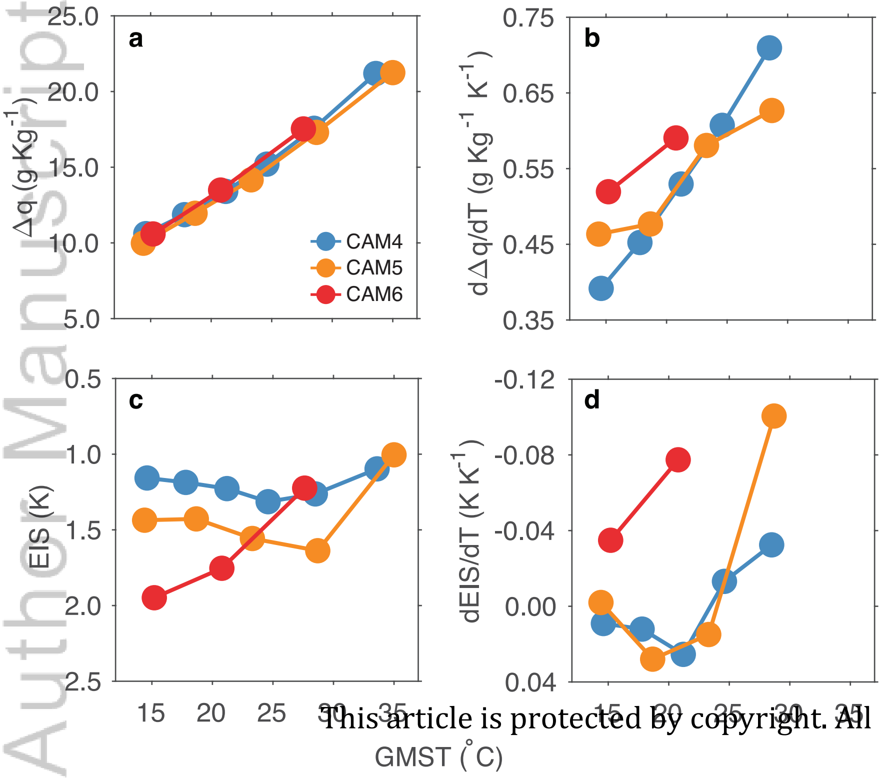
a
b
c
d
Δq (g Kg^{-1})
dΔq/dT (g Kg^{-1} K^{-1})
EIS (K)
dEIS/dT (K K^{-1})
CAM4
CAM5
CAM6
GMST (°C)